Viser Technology Pte. Ltd.
Mechanical Engineering Science
DOI: 10.33142/mes.v3i1.4335

Research Article Open Access

Embedment Effect on Eliminating Damage of CFRP Pull-riveting Process by Simulation Study

Yiqi WANG*, Zhiwei CONG, Guang XIAO, Yongjie BAO , Hang GAO

Key Laboratory for Precision and Non-traditional Machining Technology of Ministry of Education, Dalian University of Technology, Dalian, China

***Corresponding Author:** Yiqi WANG, E-mail: wangyiqi@dlut.edu.cn*

Abstract:
The rivet joints have been widely applied in aerospace and vehicle fields. During the joining process of the carbon fiber reinforced plastic (CFRP) laminates, the pre-tightening force of pulling-rivet was the key factor to ensure the connection performance. To predict the impact of clamping loads on stress and failure of laminates, the value of stress and damage evolution of the wall of a hole under the pre-tightening force were simulated by the finite element method. The results of the simulation showed that excessive clamping force led to the damage and failure of CFRP in the hole edge. Connection performance together with progressive failure process and failure modes of CFRP laminates with various pre-tightening forces were investigated. A kind of metal embedded parts embedded in the laminates was designed to reduce the damage by the simulation study. Simulation results showed that embedment reduced the failure and damage efficiently. The embedment reduced about 64% of the maximum stress.

Keywords: *embedment effect; CFRP riveted; damage evolution; damage removal*

1 Introduction

As people pay more and more attention to energy-saving and pollutant emission reduction, the demand for lightweight materials is increasing. Carbon Fiber Reinforced Polymer (CFRP) has become the preferred material for current aircraft manufacturing due to its excellent properties of lightweight and high strength. CFRP consumptions of the American Boeing 787 aircraft and the European Airbus A350XWB aircraft are more than 50%, and that of the Commercial Aircraft Corporation of China C919 aircraft reaches 12% [1-3]. In recent years, CFRP is used widely in the automotive manufacturing industry [4].

However, due to the lack of relevant theoretical methods and key technologies, the connection of composite components faces many challenges. CFRP inevitably is connected by bolting [5], riveting [6], adhesive bonding [7,8], welding [9,10], and hybrid junction [11]. Bolting is the most favorite method. The main advantages of bolting connections are easy assembly and disassembly, no special surface treatment, less environmental impact, high load carrying capacity, and high connection reliability, which is the most widely used in the aviation industry [12-15]. However, the main problems of these connection methods are destroying the integrity of the structure and having high-stress concentration around the fastener holes deteriorating joint strength, which is much more complicated and severe in CFRP laminates compared to metallic counterparts as a consequence of their inhomogeneity and anisotropy [16].

Some scholars provided much information on mechanical performance and failure mechanisms about solely bonded and riveted joints. Yang et al. [17] developed a new progressive damage model to investigate the flexural behavior and the damage evolution of CFRP laminates subjected to three-point bending. Gomez et al. proposed a simple analytical model combining spring and damper that reproduces the behavior of a structural rive joint, with less than 15% error level compared with experimental curves [18]. Simplified finite element models were also proposed to analyze stress distribution and further predicted the joint performance. Pirondi et al. [19] simulated the failure behavior of riveted joints and found that the stiffness, peak load, and energy absorption of the riveted joints agree well with the corresponding experimental results. Chowdhury et al. [20] conducted a finite element study on thin carbon fiber double lap joints. The results show that the addition of fasteners in the composite joint significantly reduces the strain energy release rate compared to the single-bond joint, thereby greatly reducing the crack propagation speed.

The researchers also studied the effect of joint

Received 20 January 2021; Accepted 23 May 2021

configuration on the mechanical properties of different joints. Sadowski et al. [21] studied the effect of the rivet arrangement geometry on the mechanical properties of riveted joints under mechanical loading. The test results show that the hybrid joints arranged with 1 + 2 type rivets are the best solution for the connection of structural members under the joint action of three kinds of rivets.

The present work aims to study the failure load and failure mode in the process of riveting in different Pre-tightening forces and how to reduce the damage in the CFRP laminates. Load-displacement curves together with peak load, energy absorption, and joint stiffness were studied. A metal embedded part was designed to reduce the failure.

2 Progressive damage model

To take into account the failure and damage of CFRP laminates effectively, a three-dimensional nonlinear progressive damage analysis model at the mesoscale level was presented. In this study, the failure criterion of the CFRP pack case was analyzed with a three-dimensional composite material failure criterion based on the Hashin-type criterion.

At first, strain and damage-free stiffness matrix based on the assumption of transverse isotropy were used to calculate the initial stress by the following equation:

$$\sigma = C^0 : \varepsilon \tag{1}$$

And then, the 3D Hashin damage criteria were as follows:

Fiber tensile failure (FT), $\varepsilon_1 > 0$:

$$\left(\frac{\varepsilon_1}{X_t/C_{11}}\right)^2 + \left(\frac{\gamma_{12}}{S_{12}/C_{44}}\right)^2 + \left(\frac{\gamma_{13}}{S_{13}/C_{55}}\right)^2 = e_{FT}^2 \tag{2}$$

Fiber compressive failure (FC),$\varepsilon_1 > 0$:

$$\left(\frac{\varepsilon_1}{X_c/C_{11}}\right)^2 = e_{FC}^2 \tag{3}$$

In-plane matrix cracking (IMT), $\varepsilon_2 > 0$:

$$\left(\frac{\varepsilon_2}{Y_t/C_{22}}\right)^2 + \left(\frac{\gamma_{12}}{S_{12}/C_{44}}\right)^2 + \left(\frac{\gamma_{23}}{S_{23}/C_{66}}\right)^2 = e_{IMT}^2 \tag{4}$$

In-plane matrix crushing (IMC), $\varepsilon_2 > 0$:

$$\left(\frac{\varepsilon_2}{Y_c/C_{22}}\right)^2 + \left(\frac{\gamma_{12}}{S_{12}/C_{44}}\right)^2 + \left(\frac{\gamma_{23}}{S_{23}/C_{66}}\right)^2 = e_{IMC}^2 \tag{5}$$

Out-of-plane matrix cracking (OMT), $\varepsilon_3 > 0$:

$$\left(\frac{\varepsilon_3}{Z_t/C_{33}}\right)^2 + \left(\frac{\gamma_{13}}{S_{13}/C_{55}}\right)^2 + \left(\frac{\gamma_{23}}{S_{23}/C_{66}}\right)^2 = e_{OMT}^2 \tag{6}$$

Out-of-plane matrix crushing (OMC), $\varepsilon_3 > 0$:

$$\left(\frac{\varepsilon_3}{Z_c/C_{33}}\right)^2 + \left(\frac{\gamma_{13}}{S_{13}/C_{55}}\right)^2 + \left(\frac{\gamma_{23}}{S_{23}/C_{66}}\right)^2 = e_{OMC}^2 \tag{7}$$

Fiber-matrix shear-out (OMC),$\varepsilon_1 < 0$:

$$\left(\frac{\varepsilon_1}{X_c/C_{11}}\right)^2 + \left(\frac{\gamma_{12}}{S_{12}/C_{44}}\right)^2 + \left(\frac{\gamma_{13}}{S_{13}/C_{55}}\right)^2 = e_{FMS}^2 \tag{8}$$

The ε_i (i=1,2,3) was normal stress, and the γ_{ij} (i,j=1,2,3; i≠j) was shear strain. The C_{ij}(i,j=1,2,3,4,5,6) was stiffness coefficient in the stiffness matrix. The S_{12}, S_{13}, S_{23} were the shear strengths of the laminate. The X_t, Y_t, Z_t represented the tensile strengths in the longitudinal direction, transverse direction, and through-thickness direction, respectively. The X_c, Y_c, Z_c represented the compressive strengths in the longitudinal direction, transverse direction, and through-thickness direction, respectively. The S_{12}, S_{13}, S_{23} were the shear strengths of the laminate.

The e was the failure factor used to characterize the damage degree of the material. For arbitrary mesh style, once $e \geq 1$, it indicated that the material had been damaged. And corresponding unit property degradation was required. There were two main ways of property degradation: one was the reduction of elastic modulus, the other was the reduction of stiffness.

3 Modeling

3.1 Specimen details

In order to verify the strengthening effect of embedment, numerical simulations on comparison of laminates without embedment and laminates with embedment were conducted. The schematic diagram of the two comparison models was shown in Fig.1. Fig. 2 showed the concrete geometries and dimensions of the riveted joint specimens. The specimens' sizes were referred to as the TB/T 1335-1996 Standard.

In order to observe the simulation results, the laminate was designed to the square and the length of the side was 100mm. The pulling rivet of LMTF and LMY type rivet sleeve was chosen in the simulation and the diameter of the pulling rivet was 16mm. The length of the rivet rob was 14mm. The contact area between the rivet head and bottom laminate was 415mm^2 and the contact area between the rivet sleeve and top laminate was 548mm^2. Clearance fit between rivet and laminate was used in the assembly, so the diameter of the central hole in the laminate without embedment was set to be 17.5mm. While the diameter of the center hole in laminates with embedment was 37.5mm. As a result of the embedment was implanted in the laminates and the embedment was stair-stepped, the diameter of the cylindrical groove in the laminates was 48mm. The thickness of laminate was 7mm with a thickness of 0.2mm per ply and the stacking sequence was (0/90)2s.

In order to enhance the connection strength between embedment and laminates, designed to be ladder-like. The diameter of the central hole in the embedment was 17.5mm. The upper half part's thickness of embedment was 4mm and the thickness of the lower half part was 3mm. The diameter of the upper ladder was 1.2 times bigger than the diameter of the pulling rivet's head. The diameter of the pulling rivet's head was 28mm, and the upper ladder's diameter was 33.6mm. The bottom ladder's diameter was 48 mm. Fig.1(c) showed the sectional view of the central area of the laminate. The contact area between the embedment and laminates used adhesive to improve the strength. In this simulation, adhesive was replaced by the tie.

3.2 Material properties

The fiber material used in finite element analysis was standard modulus woven carbon fiber T300, while matrix material was unsaturated epoxy resin E54. The properties of the CFRP laminates referred from the datasheet of Toray Company's composites were listed in Table 1, in which the parameters were from the manufacturer. Pulling rivet and rivet sleeve were both used carbon structural steel

Q235B which was widely employed in railway vehicle connection. And the property of Q235B was given in Table 2. Considering the effect of ensuring connection strength and weight loss and ensuring connection strength, the embedded part employed Al-2024-T3 and the property of which was presented in Table 3.

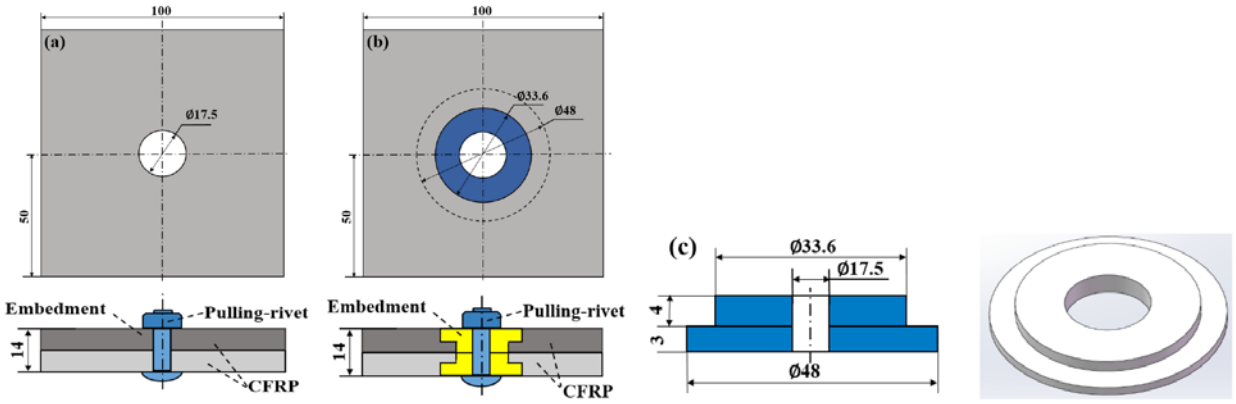

Fig.1 Geometry and dimensions of pulling riveted joint specimens: (a) CFRP laminates without embedment, (b) CFRP laminates with embedment, (c) metal embedment.

Table 1 The mechanical properties of the CFRP laminates

E1 [GPa]	E2 [GPa]	E3 [GPa]	u12	u13	u23	G12 [GPa]	G13 [GPa]	G23 [GPa]
135	8.17	8.17	0.33	0.33	0.48	4.27	4.27	2.75

Table 2 Mechanical and physical properties of Q235B

Density [g/cm3]	Tensile modulus [GPa]	Yield stress [MPa]	Tensile strength [MPa]	Poisson's Ratio
7.8	210	235	580	0.3

Table 3 Mechanical and physical properties of Al-2024-T3

Young's Modulus [GPa]	Yield Stress [MPa]	Ultimate Stress [MPa]	Poisson's Ratio
7.8	210	235	580

3.3 FE simulation

3D finite element (FE) models were established for accurate stress analyses of the specimens by the software ABAQUS 2016/Standard. Fig. 2 presented the sectional view of FE model with virtual material layers representing the rough contact surfaces. The model Ⅰ was composed of two CFRP laminates, one pulling rivet, one rivet sleeve, and model Ⅱ added two embedded parts on the basis of model Ⅰ. In order to simplify the numerical simulations and shorten the calculating time, the pulling rivet and rivet sleeves were merged into a dumbbell-shaped component.

The CFRP laminate was divided into 35 layers in the thickness direction and each ply was a single layer. The C3D8R solid elements with enhanced hourglass control were used to simulate the failure process of CFRP laminates. In order to make the calculation more accurate, the meshes of the joint-hole region were refined highly with an element size of 0.4×0.4×0.55 mm. The properties of laminates were defined by the user material. The continuum damage mechanics was implemented in ABAQUS 2016 through a UMAT subroutine for further simulation. Three contact pairs were established in the model Ⅰ, including between top laminate and bottom laminate, between the CFRP and pulling rivet, between the CFRP and rivet sleeve. In model Ⅱ, four contact pairs were established. Between top laminate and bottom laminate, between top embedment and bottom embedment, between pulling rivet and embedment, between rivet sleeve and embedment were included. In order to prevent elements interpenetration at the edges of the parts, surface-to-surface discretization was used in the contacts of various parts. In the simulation, the CFRP laminates were the master surface for the pulling rivet head-to-laminate and the surface of pulling rivet was selected as the slave surface for the rivet sleeve-to-embedment. The penalty method with hard contact, friction, small sliding, and finite sliding was used to solve the contacts. The values of frictional coefficient for laminate-to-laminate (FC1), embedment-to-embedment (FC2), pulling rivet head-to-laminate (FC3), rivet sleeve-to-laminate (FC4), pulling rivet shank-to-laminate interfaces (FC5), pulling rivet head-to-embedment (FC6), rivet sleeve-to-embedment (FC7), rivet shank-to-embedment interfaces (FC8) were 0.1, 0.3, 0.2, 0.2, 0.1 0.3,0.3,0.1 respectively, which was based on the previous experiments and studies.

Regarding the step type itself, static general analysis was used for this model. In order to apply the preload, the

bolt load plane was created in the middle of the pulling rivet. The 170 kN which was the ultimate force of pulling rivet snapped was imposed the bolted load plane. The pre-tightening force was divided into two-step to simulate fluently. The pre-tightening force was created on the propagated to the subsequent analysis step. The preload of step-1 was 1 kN and step-1 was 170 kN.

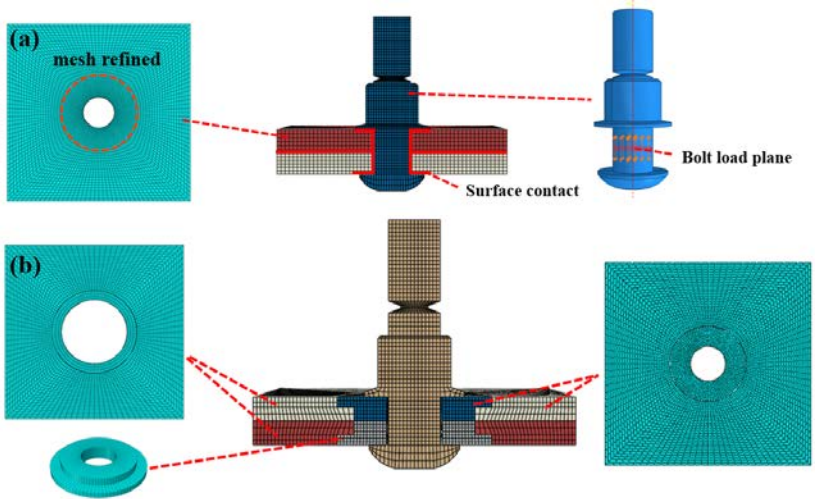

Fig.2 3D FE model of pulling riveted joint: (a) model Ⅰ: without embedment, (b) model Ⅱ: with embedment.

4 Results and discussion

The stress distribution, deformation, and damage of CFRP laminates and embedment were presented and discussed in detail. The pre-tightening force of rivet effect mechanisms was analyzed comprehensively based on the numerical results.

4.1 Stresses

4.1.1 Stresses distribution of laminates without embedment

The section view of typical stress contours around the central hole was given in Fig. 3. The critical zone for each stress component was marked by a dotted line. It could be seen from Fig. 3 and Fig. 4 that the critical zones for all stress concentrations occurred at the contact area of laminates as a result of pre-tightening force clamping, which may cause the damage and delamination of CFRP laminates. The stress S33 was taken main stress and the maximum of stress S33 was located in the contacting region between rivet and laminates because the orientation of the pre-tightening was along the Z-direction. Due to the impact of the preload from riveters, the riveting-head and the riveting sleeve-set were squeezed from both sides to the middle, stress main concentrated on the contact area. In Fig. 3(d), the value of S33 in the zone marked by the blue rectangle dotted line was negative as a result of CFRP laminates were subjected to extrusion which was opposite of the positive direction of Z-direction from pulling rivet-head and rivet sleeve. From Fig. 3(d) and Fig. 4(d), the S33 value of the red region was positive because this region expanded outward under the preload, and the expansion direction was consistent with the positive direction of the Z-direction.

The stress S11 and S22 represented respectively the stress along fiber-direction and matrix-direction. The S11 and S22 were generated because rivet contacted hardly with the hole-wall during the riveting process and the interlaminar strength of CFRP is not enough. The S11 and S12 concentrated principally in the butting area between two laminates around the central hole extended along radius direction as were depicted in Fig. 3(a) (b) and Fig. 4(a) (b). The value of S11 was higher than the value of S22 because the compressive strength of carbon fiber was lower than the matrix. The value of S12 was far lower than the value of S11 and S12 concentration areas of S12 were mainly located in the direction of 45°and -45°illustrated in Fig. 3(c) and Fig. 4(c).

Because of the ply orientation effect, the critical zones of stress were non-uniform in the laminates. In order to describe visually stress distribution around the fastener hole, some paths were set in the radius, thickness, and circumference direction. The thickness and circumference direction path was created at the contacting area between upper laminate and lower laminate. Fig. 5(a) gave the relative Mises stress along the thickness path, which was the bottom of the lower plate to the top of the upper plate along the central hole-wall. It could be seen that the radial stress was almost symmetric. It indicated that the maximum position of stress was located in the contact area between the laminates and the stress gradually decreased from the middle to both sides, which was accordant with the Figs. 3(a-c). Fig.5 (b) showed the variation of stress along the radius direction. The numerical results showed that stress was continuous. The stress curves of the bottom side of the upper laminate and the top side of the lower laminate were coincident. As the radius increased, the stress decreased gradually. When the distance from the hole wall was 10mm, the stress reduced to the safe zone. The stress of circumferential direction was depicted in Fig.5 (c), the maximum stress was at the edge of the hole wall and the stress of circle direction decreased with circumferential expanding. The stress variation trend was almost consistent with Fig.5 (c).

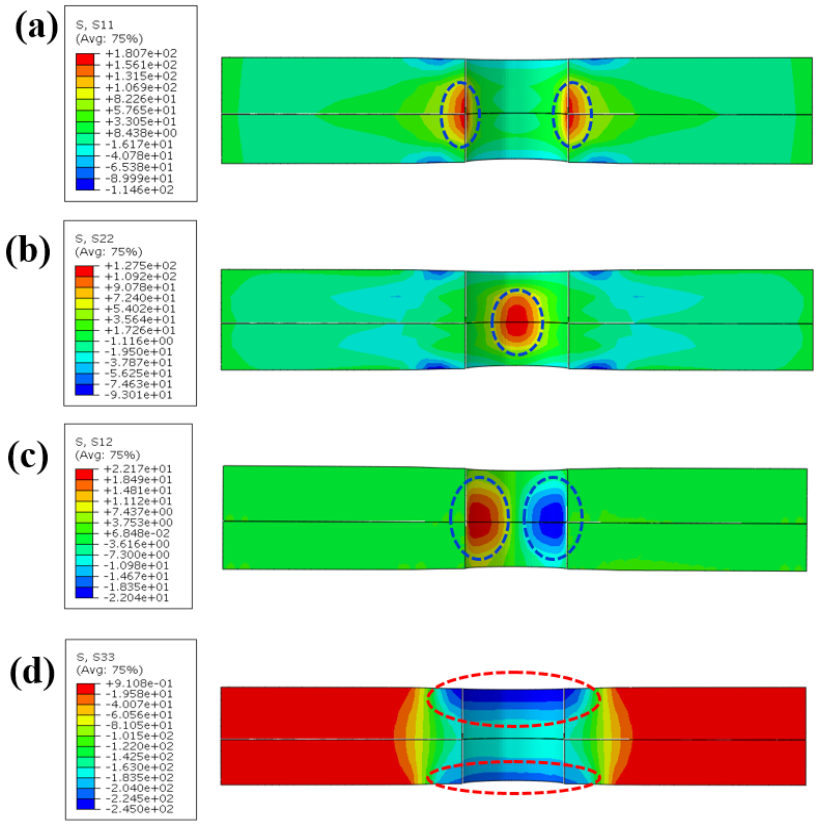

Fig.3 Stress profile view of laminate without embedment: (a) S11, (b) S22, (c) S12 (d) S33.

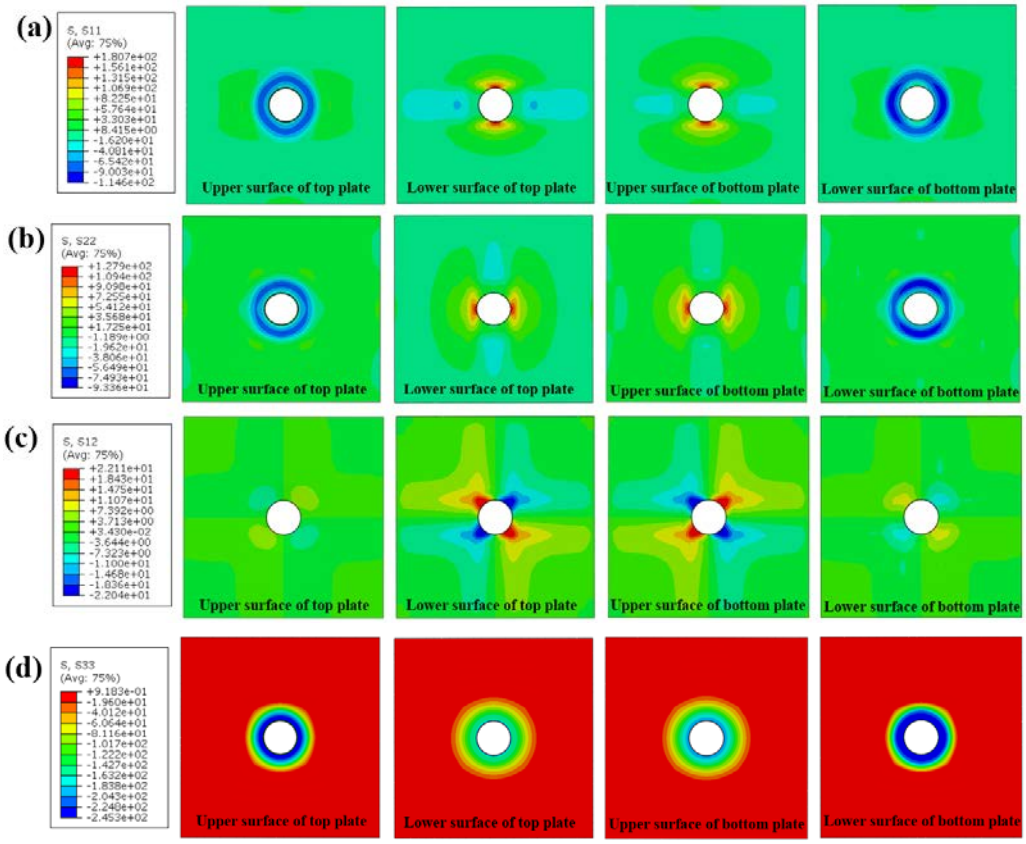

Fig.4 Surface stress distribution diagram of laminates without embedment in different directions: (a) S11, (b) S22, (c) S12, (d) S33.

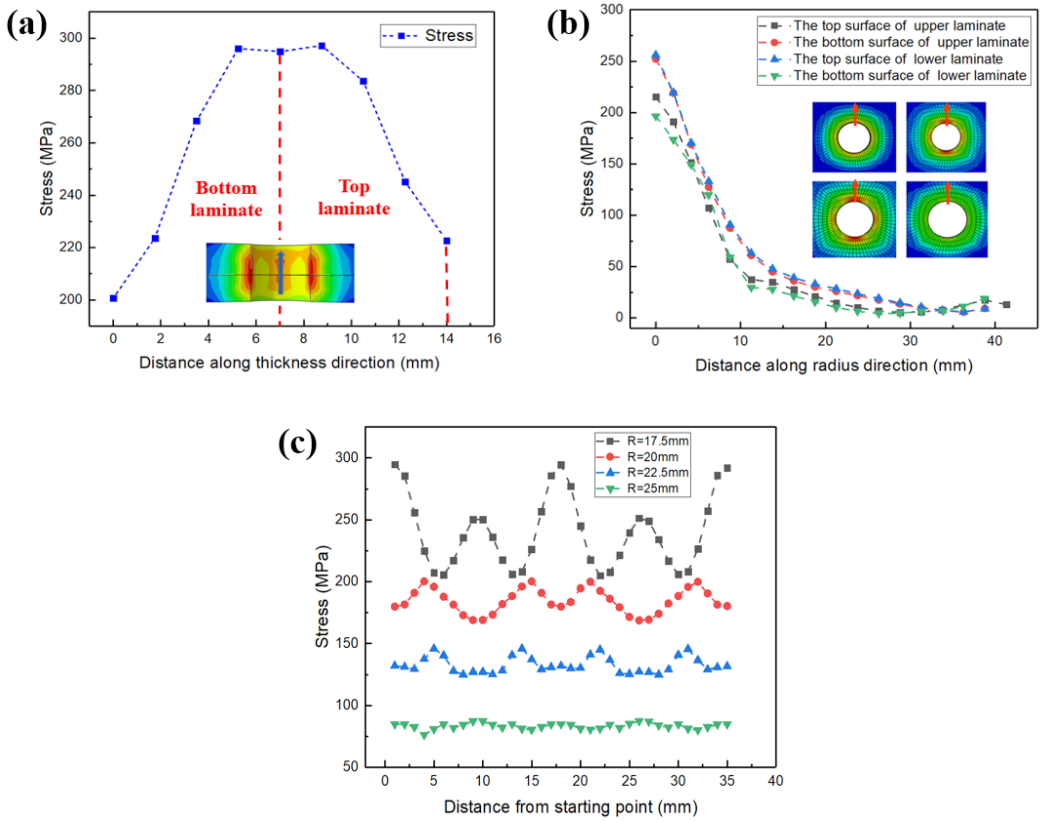

Fig.5 The stress of laminates without embedment along various paths: (a) stress along the thickness direction, (b) stress along radius direction, (c) stress along circumference direction.

4.1.2 Stresses distribution of laminates without embedment

Fig. 6 and Fig. 7 presented the stress distribution of laminates with embedment. The maximum pressure was 56.87 MPa, which didn't exceed the fiber and matrix strength. Thus there wasn't damage to the laminates. As depicted in Fig. 6(a) and (b), the stress S11 and S22 were distributed symmetrically along the X-axis and Y-axis respectively. The stress concentration mainly occurred on the upper area of the bottom laminate, which was due to the pressure from the rivet head-side larger than the pressure from the rivet nut-side. And the frictional force between the two laminates could lead to the stress concentration area. In Figs. 6 (a-b) and Figs. 7 (a-b), the stress of the blue region was negative because this area existed internal tension which was generated during riveting and the direction of tension was opposite from the positive direction of the X-axis and Y-axis. The inner tension expanded from the central hole to the side of the laminates and decreased gradually. The value of stress S12 was too small to affect the whole stress distribution from Fig. 6 (c) and Fig. 7(c). The stress S33 has distributed the direction of 45°and -45°, and the stress was small extremely.

The stress of laminates with embedment along various paths is illustrated in Fig. 8.

4.1.3 Stress distribution of embedment

Fig. 9 showed the stress distribution of the embedded part. The maximum stress was 431.3 MPa, which was far less than the ultimate load of aluminum. So using metal embedded parts could offset contact main contact stress thus reducing the damage of CFRP. From Figs. 9(a-c), the surface stress spread radially from the central hole to the sides, which was verified in Fig. 10. In Fig. 9(d), the position of maximum stress was located in the lower region of the bottom laminate as a result of the hard contact between the bottom laminate and pulling rivet-head.

To present the path effect on the stress distribution, the stresses along the radius and thickness direction of laminates were plotted in Fig. 10. In the radius direction, the stress decreased with the radius increased from the center hole. In Fig. 9(b), zone A was the stress concentration area and zone B was the safety region and the area of safety was more than half of the area of embedded parts, so the embedment could sure that large values of stress were not transferred to the laminates. In the thickness direction, there was little difference in stress, which indicated contact stress distribution of embedded part was homogenous.

4.2 Local deformations of laminate around the rivet hole

Fig. 11(a) gave the deformations of laminates without laminates. The maximum deformation was the same position as the maximum stress. On the whole, the deformation of the lower plate was greater than the upper plate as illustrated in Fig. 11(a), which was the pressure from the rivet-head was higher than the pressure from the rivet-sleeve. In the clamping loading process, the top laminate's deformation increased slower than the bottom laminate.

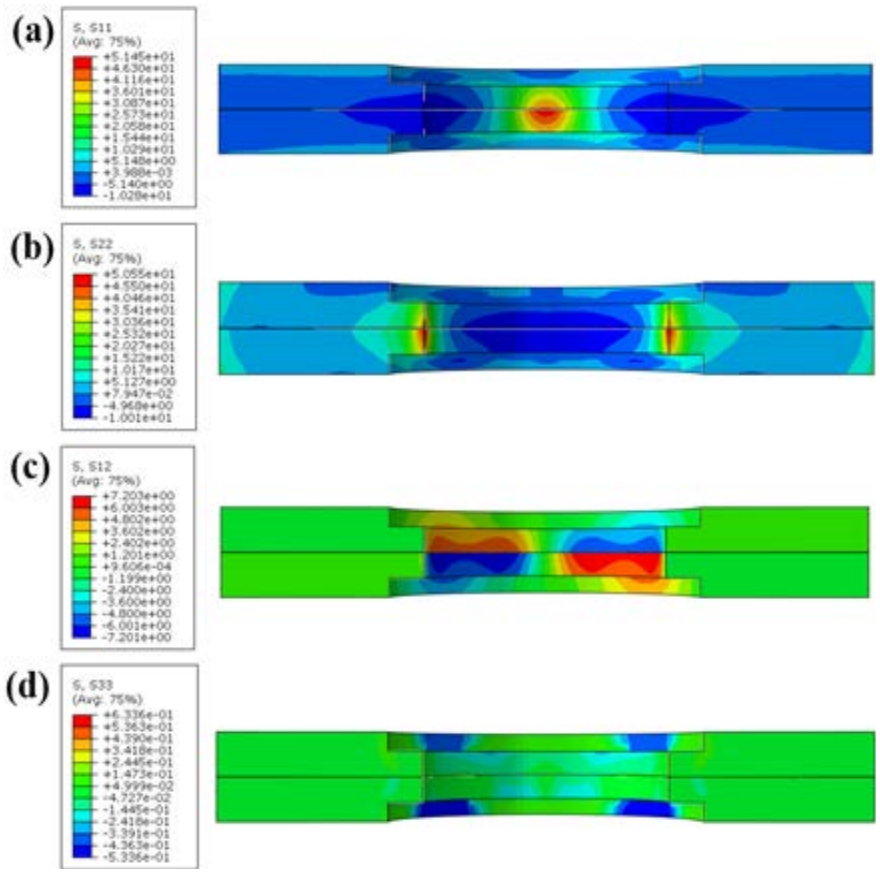

Fig.6 Stress profile view of laminate with embedment: (a) S11, (b) S22, (c) S12, (d) S33.

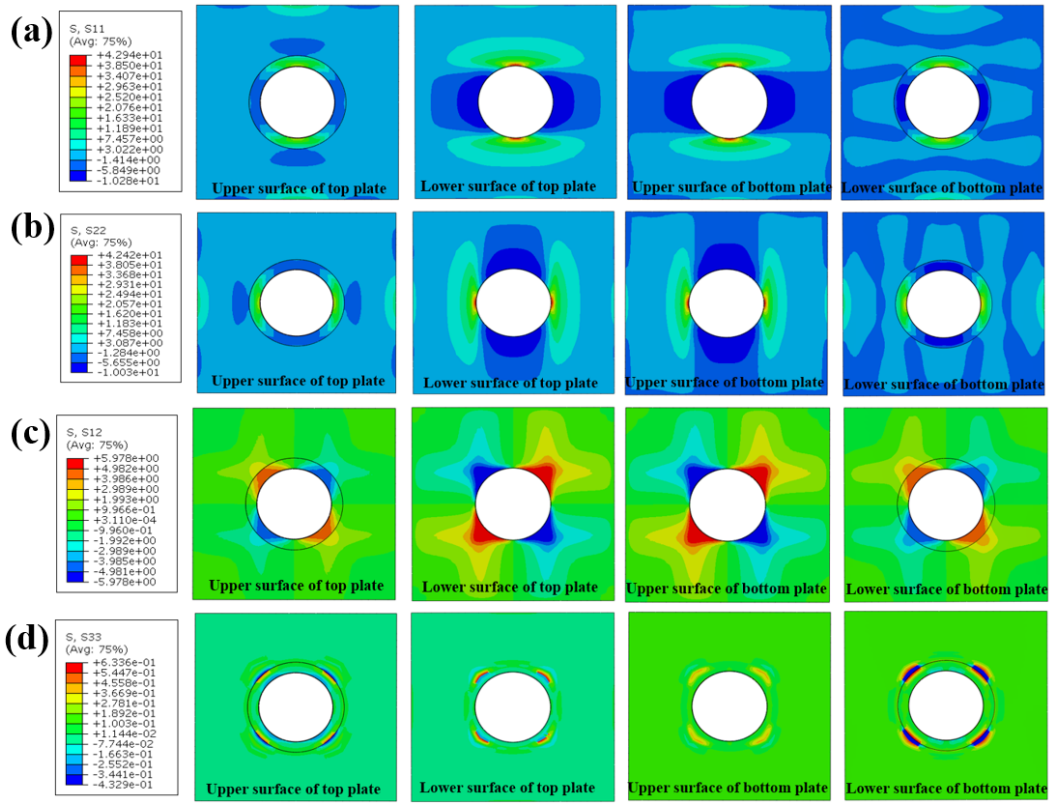

Fig.7 Surface stress distribution diagram of laminates with embedment in different directions: (a) S11, (b) S22, (c) S12, (d) S33.

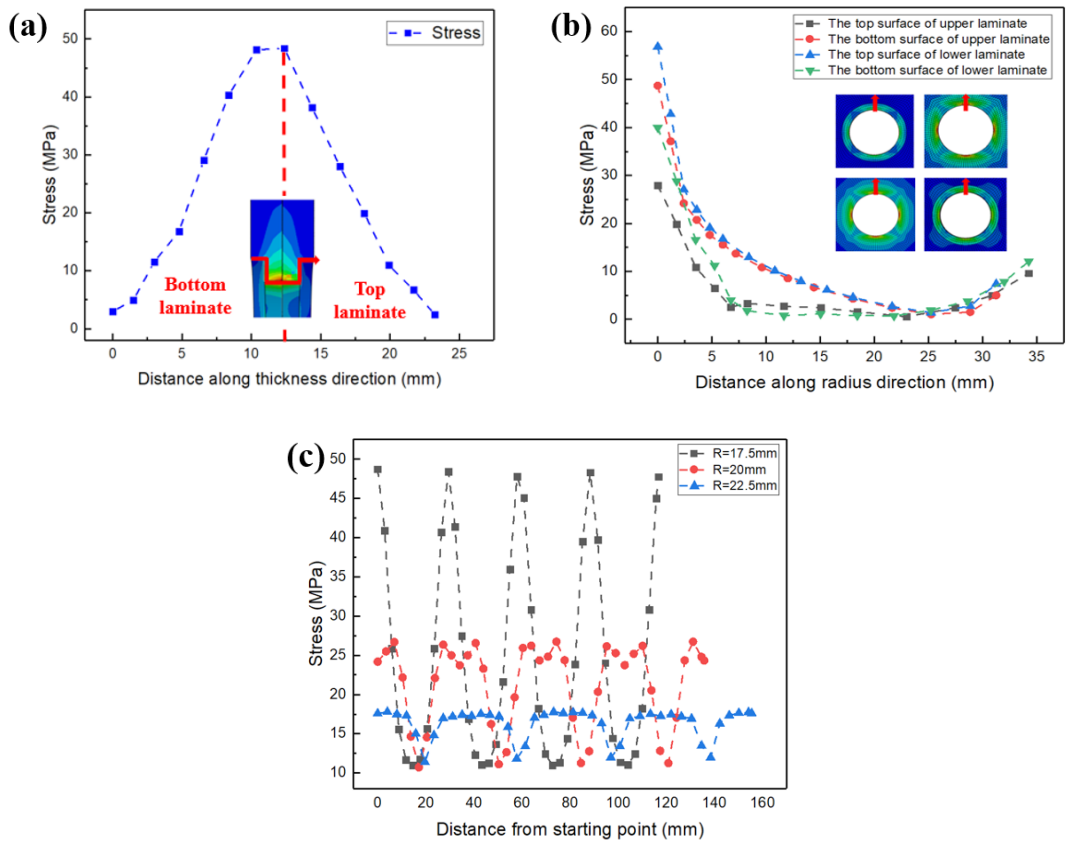

Fig.8 The stress of laminates with embedment along various paths: (a) stress along thickness direction, (b) stress along radius direction, (c) stress along circumference direction.

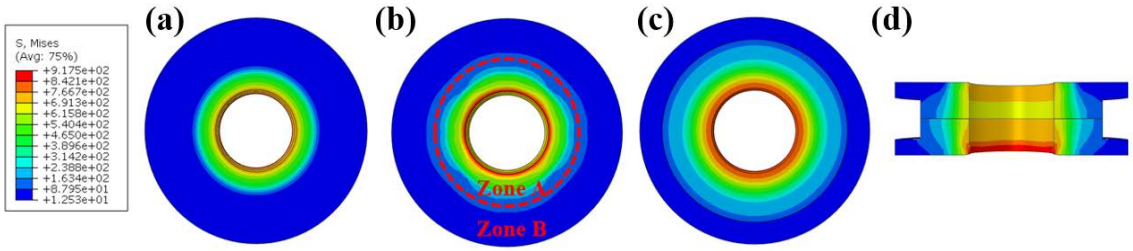

Fig.9 The stress of embedment: (a) top surface, (b) bottom surface, (c) contact surface of two laminates, (d) profile view of embedment.

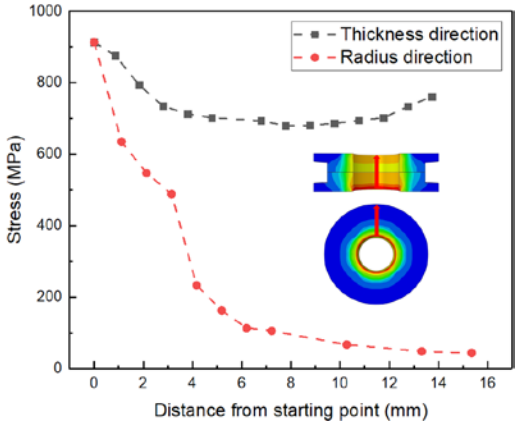

Fig.10 Stress distribution of embedment along a different path.

The top laminate contacting with rivet sleeve and bottom laminate contacting with pulling rivet-head was sinking due to clamping action from the pre-tightening force. The sinking direction was towards the middle. In the meanwhile, warping deformation occurred on the sides of laminates. In Fig. 11(b), the deformation of each position in the laminates was far less than the laminates without embedment. The maximum deformation position didn't occur in the central hole because the embedment bears most of the deformation. The sides of laminates with embedment also had warping deformation, but the value of deformation far lower than the deformation of laminates without embedment. Zone D exhibited a negative deformation state since the deformation direction was towards the negative direction of the z-axis, while the deformation of zone C was positive because the deformation direction with the z-axis's positive direction was consistent.

The deformation along different paths was shown in Fig.12. From Fig. 12, we could see the distance between top laminate and bottom laminate getting larger and larger as the distance increased. The schematic diagram of riveting finished was shown in Fig. 14. Due to the clamping force, there was a gap between the two plates. It could be seen that the radial deformation of the first half changed almost linearly from Fig.12 (a), which indicated that the deformation of the first half was uniform. And the curves of laminates along the radius were almost symmetric. For top laminate, the largest relative radial deformation was smaller than bottom laminate. The maximum distances of laminates without embedment and laminates with embedment were 0.11mm and 0.022mm respectively illustrated in Fig. 12. The value of the maximum distance between laminates decreased by 80%. Thus it could be seen that embedment played a significant role in reducing layer deformation.

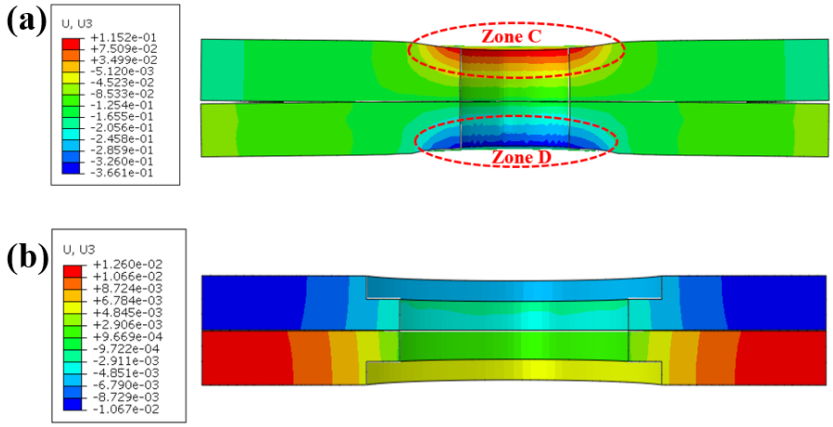

Fig.11 Relative deformation of laminates: (a) without embedment, (b) with embedment.

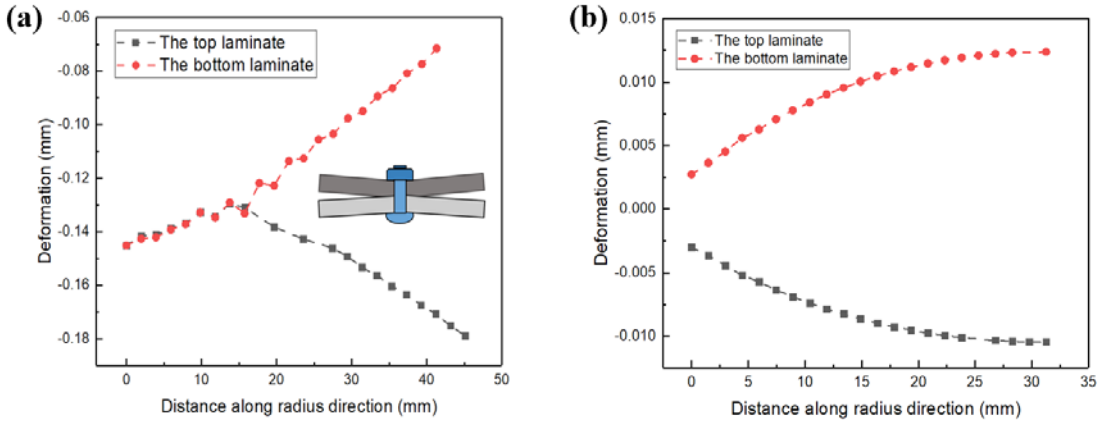

Fig.12 Relative deformation of contact area between top laminate and bottom laminate: (a) without embedment, (b) with embedment.

4.3 Local damages of laminate around the rivet hole

The damage of laminates without embedment is illustrated in Fig. 13. It could be observed that damage occurs near the wall of the hole due to the stress concentration feature and the hole was radially compressed and expanded circumferentially. Fiber and matrix compressive damage generated initially closed to the surface of laminates due to contact stress between laminates and fasteners. Damage extended afterward to the contact area of the two plates along the hole wall until the pulling riveting process was

completed. The variation trend of in-plate damage was consistent with the variation of stress. In contrast, there wasn't damage in the CFRP laminates with embedment due to the embedment took most of the stress from Fig. 13. The embedment could inhibit the damage of CFRP laminates during the riveting process.

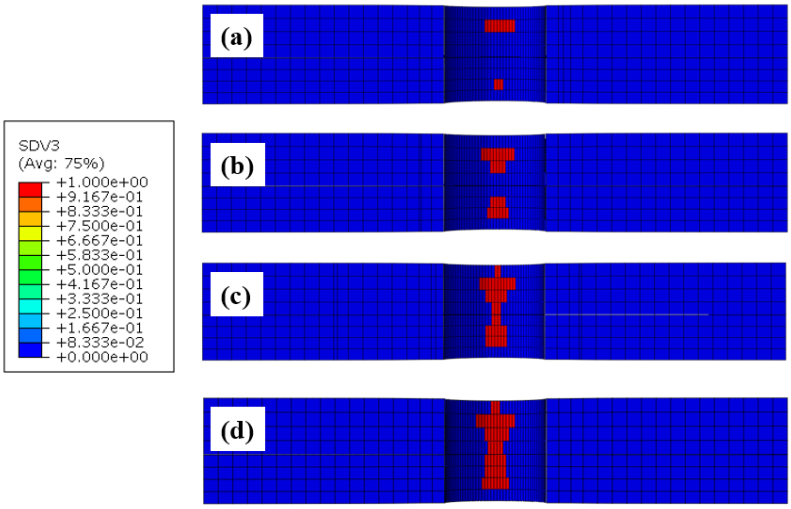

Fig.13 Progressive failure evolution of laminates: (a) damage initiation, (b) ultimate load, (c) damage propagation, (d) failure.

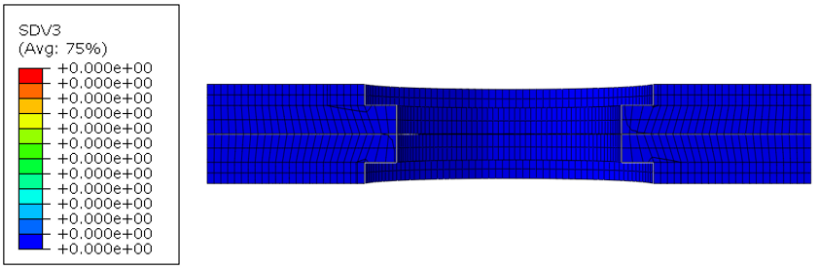

Fig.14 Damage condition of laminates with embedment.

5 Conclusions

This paper investigated the stress, deformation, and failure mechanism of pulling riveted joints when connecting CFRP laminates. The simulation results could be applied to the automotive industry to improve the mechanical properties and reliability of CFRP, which also helped to further understand the progressive failure process and fracture mechanism of CFRP-CFRP joints made with different joining methods and design parameters. The following conclusions can be drawn from the above study.

(1) During the pulling riveting process, stress concentration occurred close to the central hole and led to the failure of the laminates as a result of excessive clamping force.

(2) The simulation results showed that embedment embedded in the CFRP laminates reduced the stress concentration and damage near the hole-wall. About 64% of the maximum stress was reduced by using the designed embedment.

(3) Progressive failure process of riveted joint indicated that clamping load led to crack initiation and propagation on the edge of the hole of CFRP laminates. Fracture of the adhesive layer was predicted before the mechanical failure of the rivet.

References

[1] V Krishnaraj, R Zitoune, F Collombet. Comprehensive review on drilling of multi material stacks. J Mach Forming Technol 2010(2):1–32.

[2] C Campbell. Structural assembly. In: Campbell FC,. Manufacturing technology for aerospace structural materials. Oxford: Elsevier Science; 2006.

[3] Y Rhee, J Yang. A study on the peel and shear strength of aluminum/CFRP composites surface-treated by plasma and ion assisted reaction method. Compos Sci Technol 2003(63):33–40.

[4] F. Lambiase, D Ko. Feasibility of mechanical clinching for joining aluminum AA6082- T6 and Carbon Fiber Reinforced Polymer sheets, Mater. Des. 2016 (107): 341–352.

[5] J Hu, K Zhang, Q Yang, H Cheng, S Liu, Y Yang. Fretting behavior of interference between CFRP and coated titanium alloy in composite interference-fit joints under

service condition. Mater Des 2017 (134):91–102.
[6] F Lambiase. Mechanical behavior of polymer-metal hybrid joints produced by clinching using different tools. Mater Des 2015(87):606–18.
[7] T Kim, J Kweon, J Choi. An experimental study on the effect of overlap length on the failure of composite-to-aluminum single-lap bonded joints. J Reinf Plast Comp 2008; 27(10):1071–81.
[8] N Tsouvalis, V Karatzas. An investigation of the tensile strength of a composite-to-metal adhesive joint. Appl Compos Mater 2011, 18(2):149–63.
[9] J Esteves, S Goushegir, J Santos, et al. Friction spot joining of aluminum AA6181-T4 and carbon fiber reinforced poly (phenylene sulfide): effect of process parameters on the microstructure and mechanical strength. Mater Des 2014, 66(4):437–45.
[10] B Frank, W Guntram, E Dietmar. Ultrasonic metal welding of aluminium sheets to carbon fibre reinforced thermoplastic composites. Adv Eng Mater 2010, 11(1–2):35–9.
[11] F Smith. An innovation in composite to metal joining. Mater Process Rep 2004, 20(2):91–96.
[12] A Pisano, P Fuschi. Mechanically fastened joints in composite laminates: Evaluation of load bearing capacity [J]. Composites Part B: Engineering, 2011, 42(4):949-961.
[13] F Irisarri, F Laurin, N Carrere, et al. Progressive damage and failure of mechanically fastened joints in CFRP laminates – Part I: Refined Finite Element modelling of single-fastener joints [J].Composite Structures, 2012, 94(8):2269-2277.
[14] T Qin, L Zhao, J Zhang. Fastener effects on mechanical behaviors of double-lap composite joints [J]. Composites structures, 2013(100):413-423.
[15] A Pramanik, A K. Basak, Y Dong, et al. Joining of carbon fibre reinforced polymer (CFRP) composites and aluminium alloys – A review [J]. Composites Part A: Applied Science and Manufacturing, 2017(101):1-29.
[16] G Lim, K Bodjona, K Raju, S Fielding, V Romanov, L Lessard. Evolution of mechanical properties of flexible epoxy adhesives under cyclic loading and its effects on composite hybrid bolted/bonded joint design, Compos. Struct. 2018 (189) :54–60.
[17] Y Yang, X Liu, Y Wang, et al. A progressive damage model for predicting damage evolution of laminated composites subjected to three-point bending. Composites Science and Technology 2017 (151):85-93.
[18] S Gómez, J Oñoro, J Pecharromán. A simple mechanical model of a structural hybrid adhesive/riveted single lap joint, Int. J. Adhes. Adhes. 2007 (27) 263–267.
[19] A Pirondi, F Moroni. Clinch-bonded and rivet-bonded hybrid joints: application of damage models for simulation of forming and failure, J. Adhes. Sci. Tech. 23 (2009) 1547–1574.
[20] N Chowdhury, J Wang, W Chiu, P Chang. Experimental and finite element studies of thin bonded and hybrid carbon fibre double lap joints used in aircraft structures, Compos. Part B-Eng. 2016 (85):233–242.
[21] T Sadowski, E Zarzeka-Raczkowska. Hybrid adhesive bonded and riveted joints – influence of rivet geometrical layout on strength of joints, Arch. Metall. Mater. 2012 (57):1127–1135.